analyses may be acceptable at entry velocities of 8 km/sec or less.

The spectral flux distribution from the continuum and molecular bands and the line transitions for trajectory C are shown in Fig. 2. The radiation code of Ref. 5 uses the "line grouping" technique and as shown in part a by the results, the absorption of radiation in the boundary layer occurred at photon energies of 7.1, 8.4, and 9.4 ev. The majority of the lines in these groups are neutral carbon atoms. For the continuum and molecular contributions (part b), the absorption of the radiation in the boundary layer occurred at photon energies greater than 7 ev. The results from trajectories A and B (not illustrated here) showed that the molecular band systems, primarily CN and $CO(4^+)$, dominated the spectrum at the lower velocities. The predominant absorption in the boundary layer was the absorption of the $CO(4^+)$ transition in the 7–10 ev range. At the higher velocities, the atomic and ionic species continuum and lines were more important. Also at the higher velocities there was significant absorption of the ultraviolet by the carbon species.

The steady-state ablation rates were calculated during the boundary layer solutions and were not arbitrarily prescribed. Hence, they should be representative of the rates actually experienced by a Venusian entry vehicle during peak radiative heating. In all cases studied, the mass injection would be termed "moderate blowing" and there was still significant convective heating.

Concluding Remarks

A method for the calculation of the stagnation region, radiative flowfield with steady-state ablation has been described and results presented for peak heating conditions during typical Venusian entries. The ablation material considered was high-density phenolic nylon. The results of these calculations show that, at entry velocities around 10 km/sec, reasonable estimates of stagnation region radiative heating during Venusian entry may be obtained by relatively simple analyses which ignore nonadiabatic effects in the shock layer and the absorption of shock layer radiation by ablation products. At higher entry velocities, however, the assumption of an isothermal slab has been shown to lead to significant overprediction of radiation to the wall from the inviscid shock layer, and the injection of ablation products has been shown to significantly reduce the radiative heating. At the lower velocities (< 10 km/sec) acceptable estimates of radiative heating may be obtained by including a nonablating boundary layer. At the highest velocities studied, ablation product injection must be accounted for, but acceptable results may be obtained from a simplified analysis that assumes that the ablation products have the same composition as the Venusian atmosphere.

References

[1] Garrett, L. B., "An Implicit Finite Difference Solution to the Viscous Radiating Shock Layer With Strong Blowing," Ph.D thesis, 1971, North Carolina State Univ. at Raleigh, Raleigh, N.C.

[2] Wilson, K. H., "Massive Blowing Effects on Viscous, Radiating, Stagnation-Point Flow," AIAA Paper 70-203, New York, 1970.

[3] Falanga, R. A. and Sullivan, E. M., "An Inverse-Method Solution for Radiating, Nonadiabatic, Equilibrium Inviscid Flow Over a Blunt Body," TN D-5907, 1970, NASA.

[4] Barlett, E. P. and Kendall, Robert M., "An Analysis of the Coupled Chemically Reacting Boundary Layer and Charring Ablator," CR-1062, 1968, NASA.

[5] Nicolet, W. E., "Advanced Methods for Calculating Radiation Transport in Ablation-Product Contaminated Boundary Layers," CR-1656, 1970, NASA.

[6] Jaworski, W. and Nagler, R. G., "A Parametric Analysis of Venus Entry Heat-Shield Requirements," TR 32-1468, 1970, Jet Propulsion Lab., Pasadena, Calif.

[7] Deacon, H. J. Jr. and Rumpel, W. F., "Radiative Transfer Properties of a Shocked Venus Model Atmosphere," *Journal of Spacecraft and Rockets*, Vol. 8, No. 2, Feb. 1971, pp. 177–182.

Approximate Method for Calculating Heat Transfer to Yawed Cylinders in Laminar Flow

SHOICHI SAYANO* AND GEORGE F. GREENWALD†
McDonnell Douglas Astronautics Company—West, Huntington Beach, Calif.

Nomenclature

D = diameter at the measurement location
h = heat-transfer coefficient
K = coefficient defined by Eq. (4)
M = Mach number
P = pressure
$\dot{q}$ = heat-transfer rate
R = radius at the measurement location, $D/2$
Re_D = Reynolds number based on diameter
T = temperature
x = axial distance along cylinder
λ = yaw angle
μ = viscosity

Subscripts

FP = flat-plate value
t = stagnation condition behind a normal shock
$\lambda = 0$ = zero-yaw value
∞ = freestream value
s = value at stagnation line of yawed cylinder
N = normal component

Introduction

THE current method of evaluating heat transfer to the cylindrical section of a supersonic vehicle at angle of attack often requires utilization of two separate calculations: the tangent-cone method is used at small angles of attack, while an empirical yawed-cylinder technique is employed at larger angles. The tangent-cone and yawed-cylinder equations are not generally compatible and may yield different heating rates at the same vehicle angular orientation. As a result, the heating rate history can be highly discontinuous at the switchover point between equations. A new empirical equation has been developed for laminar flow which eliminates the two-step calculation and provides a continuous solution for stagnation-line heat-transfer coefficient at any angle of attack; it also satisfies the flat-plate solution at zero angle of attack. The equation is a modification of the $\cos^{1.5}\lambda$ relationship and is based on wind-tunnel data from a variety of cylindrical models. This Note discusses the development of the new empirical correlation and presents the resulting improvement in the method for calculating stagnation-line heat transfer at angles of attack.

Analysis

The laminar heat-transfer coefficient along the stagnation line of a yawed cylinder was shown by Beckwith and Gallagher[1] to simplify, for $M_{N\infty} \gg 1$ to

$$h/h_{\lambda=0} = (T_t/T_s)^{1/4}(P_s/P_t)^{1/2}(\mu_s/\mu_t)^{1/2} \quad (1)$$

which leads to

$$h/h_{\lambda=0} = \cos^n\lambda \quad (2)$$

Received September 1, 1972; revision received October 13, 1972.
Index categories: Boundary Layers and Convective Heat Transfer—Laminar; Supersonic and Hypersonic Flow; Rocket Vehicle Aerodynamic Heating.

* Senior Engineer/Scientist, Advanced Aero/Thermodynamics and Nuclear Technology, Advanced Systems and Technology. Associate Member AIAA.

† Senior Engineer/Scientist, Delta/MLV Aero/Thermodynamics Section, Flight Mechanics Department, Development Engineering. Member AIAA.

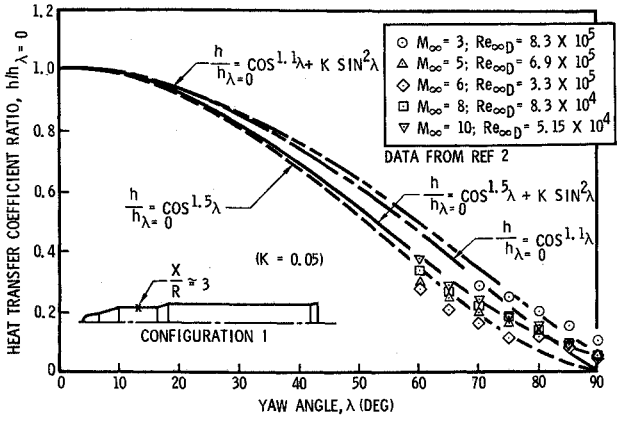

Fig. 1 Heat-transfer variation with yaw angle—Configuration I.

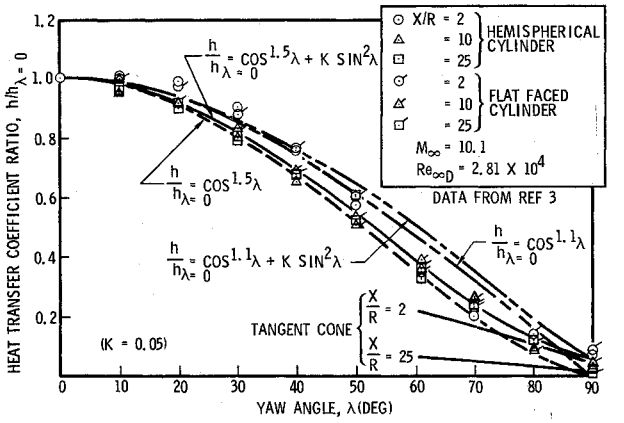

Fig. 3 Heat-transfer variation with yaw angle for 1.25-in.-diam cylinder.

where $n = 1.5$ for a linear viscosity-temperature relation, and $n = 1.1$ if Sutherland's viscosity-temperature law is used.

Previous correlations have indicated good agreement between Eq. (2) and experimental data at high angles of attack (low yaw angle). At zero angle of attack, however, Eq. (2) predicts zero heating while the data naturally correspond to flat plate heating values.

A modification to Eq. (2) is proposed to account for effects of zero angle-of-attack heating in the following way

$$h/h_{\lambda=0} = \cos^n\lambda + K \sin^2\lambda \tag{3}$$

where $n = 1.5$ or 1.1, depending on the viscosity law used, and K is an adjustable coefficient equal to the normalized flat plate heating rate

$$K = \dot{q}_{FP}/\dot{q}_{\lambda=0} \tag{4}$$

At small values of λ (high angle of attack) the first term of Eq. (3) dominates, while at large values of λ (small angles of attack) the second term becomes significant. Equation (3) therefore provides a means of fitting the experimental data throughout the entire range of angle of attack from 0 to 90°. Note that the heat-transfer coefficients in Eq. (3) are normalized with respect to the stream total temperature.

Comparison with Experimental Data

Four sets of experimental data were reviewed from wind-tunnel tests of missile scaled models and simple swept cylindrical bodies. To provide a common means of evaluation, all data were normalized with respect to the stagnation-line heat-transfer value for unswept cylinders, in general, as obtained from Beckwith and Gallagher.[1] However, if measurements at zero yaw angle ($\lambda = 0$) were available, the measured values were used.

Figures 1 and 2 present the stagnation-line heat-transfer data obtained for two Agena configurations[2] using the thin-skin heat-transfer measurement over the range of Mach number from 3 to 10 and angle of attack from 0 to 30°. Figure 3 presents the stagnation-line heat-transfer data for hemispherical and flat-faced cylinders at Mach 10, (Ref. 3). Additional data at $M = 10$ and $Re_D = 5.6 \times 10^4$ (not presented) from Ref. 3 gave similar agreement. Figure 4 shows the stagnation-line heat-transfer data from Refs. 4 and 5, as well as two sets of unpublished data; the first, from flat-faced cylinders at $M \sim 25$, and the second from wind-tunnel experiments on a missile body conducted at Mach 8.

The data presented in Figs. 1–4 are compared with Eq. (2) and the proposed empirical curve fit of Eq. (3) for both exponents considered. The value of the constant K varies with the location on the vehicle and the flat-plate heating theory used; however, for simplicity a constant value of 0.05 was used. It is evident that Eq. (3), with $n = 1.5$, provides an excellent fit to the data and can define heating on a cylindrical body continuously throughout all angles of attack.

Since it is customary to use tangent-cone theory to define heating rates at low angles of attack, the tangent-cone values for the conditions of Ref. 3 at two x/R locations were also calculated, and are presented in Fig. 3. At $x/R = 2$, flat-plate heating is identical to the value predicted by Eq. (3) (i.e., $K = 0.05$). As the angle of attack increases (yaw angle decreases) Eq. (3) and the tangent-cone solution continue to provide nearly identical results for up to several degrees of change. The two equations deviate significantly after approximately 10° angle of attack at an $x/R = 2$. However, as expected, the tangent-cone theory deviates more rapidly from both the data and Eq. (3) at larger values of x/R.

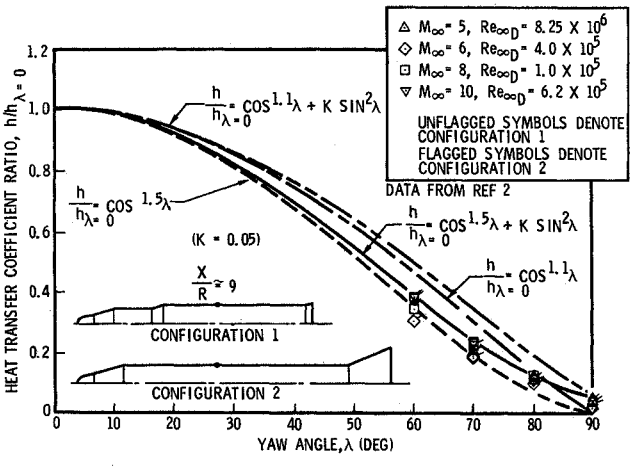

Fig. 2 Heat-transfer variation with yaw angle—Configurations I and II.

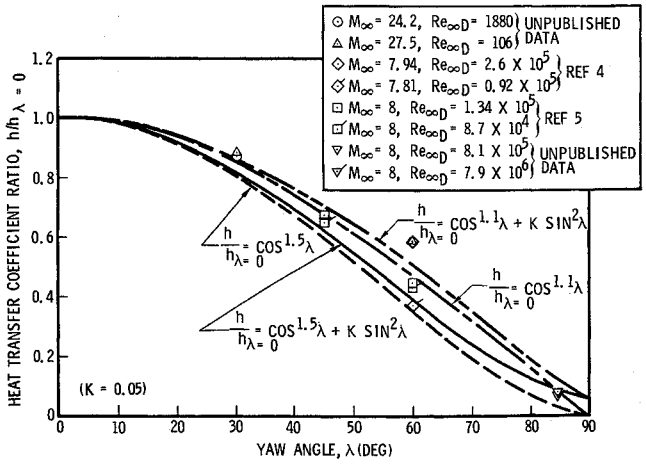

Fig. 4 Heat-transfer variation with yaw angle on cylinders in laminar flow.

Conclusions

The proposed empirical equation for stagnation-line heating on a cylinder in laminar flow agrees with flat-plate heat-transfer values at zero angle of attack ($\lambda = 90°$), and provides a smooth transition from the flat-plate value to the yawed-cylinder solution. Comparisons with wind-tunnel data indicate excellent agreement at all angles of attack when an exponent of 1.5 is assumed for the first term. At small angles of attack, the equation also agrees with the often-used tangent-cone solution, and eliminates some of the previous limitations with yawed-cylinder techniques.

References

[1] Beckwith, I. E. and Gallagher, J. J., "Local Heat Transfer and Recovery Temperatures on a Yawed Cylinder at a Mach Number of 4.15 and High Reynolds Numbers," TR R-104, 1961, NASA.

[2] Laden, G. M., Dennis, J. R., and Liskovec, J. C., "The Effects of Angle of Attack on the Ascent-Phase Aerodynamic Heating of Agena Vehicles," Lockheed Rept. LMSC A838943, Feb. 1967, Lockheed Missile and Space Co., Sunnyvale, Calif.

[3] Bergquaum, J. E., "Aerodynamic Heating Investigation on Cylindrical Configuration in AEDC Tunnel C (R-128)," Lockheed Rept LMSC 805538, Nov. 1965, Lockheed Missile and Space Co., Sunnyvale, Calif.

[4] Hunt, J. L., Bushnell, D. M., and Beckwith, I. E., "The Compressible Turbulent Boundary Layer on a Blunt Swept Slab With and Without Leading-Edge Blowing," TN D-6203, March 1971, NASA.

[5] Bushnell, D. M., "Interference Heating on a Swept Cylinder in Region of Intersection With a Wedge at Mach Number 8," TN D-3094, Dec. 1965, NASA.

Material Design Concepts for Filament-Wound, Graphite-Graphite Heatshields: Further Analysis

TOMMY R. GUESS*
Sandia Laboratories, Albuquerque, N.Mex.
AND
CHARLES W. BERT†
University of Oklahoma, Norman, Okla.

Introduction

IN a previous paper[1] by the present authors, the thermal stress equations contained an algebraic error. Also, the shear coupling effect was not included. The combination of these two effects significantly affects the numerical results presented. The purpose of this Engineering Note is to list the equations resulting from a new derivation with shear coupling included and to present and discuss new numerical results for each material design concept considered in Ref. 1. More up-to-date material properties are used in the present analysis.

Received September 12, 1972. This work was supported by the U.S. Atomic Energy Commission. The authors thank C. S. Hoyle of Sandia Laboratories, Livermore, Calif. for pointing out discrepancies in Ref. 1, and R. C. Reuter Jr. of Sandia Laboratories, Albuquerque, N. Mex. for helpful discussions and for making his computer code available.

Index categories: Structural Composite Materials (including Coatings); Thermal Stresses.

*Member of Technical Staff, Composites Research and Development.

†Professor and Director, School of Aerospace, Mechanical and Nuclear Engineering. Associate Fellow AIAA.

Stress Distribution Equations

The equations listed below (these include the shear coupling effect) replace Eqs. (A2–A11) of Ref. 1. The same assumptions of a balanced layup and of quasi-homogeneity through the thickness were used in the derivation. However, the bending-stretching coupling (B_{ij}) effects resulting from temperature-dependent property variation through the thickness are included. The in-plane normal and shear stresses as a function of axial and radial position in the shell are

$$\sigma_1(x,z) = N_{T1}\Delta[A_{22}Q_{11}(z) - A_{12}Q_{12}(z)] + N_{T2}\Delta[A_{11}Q_{12}(z) - A_{12}Q_{11}(z)] + [M_{T1}^*/(2R\delta^2 A_{11}D_{11}^*)] \times [A_{12}Q_{11}(z) - A_{11}Q_{12}(z)]\psi(x) + (M_{T1}^*/D_{11}^*)zQ_{11}(z)\phi(x) - \beta_1(z)T(z) \quad (1)$$

$$\sigma_2(x,z) = N_{T1}\Delta[A_{22}Q_{12}(z) - A_{12}Q_{22}(z)] + N_{T2}\Delta[A_{11}Q_{22}(z) - A_{12}Q_{12}(z)] + [M_{T1}^*/(2R\delta^2 A_{11}D_{11}^*)] \times [A_{12}Q_{12}(z) - A_{11}Q_{22}(z)]\psi(x) + (M_{T1}^*/D_{11}^*)zQ_{12}(z)\phi(x) - \beta_2(z)T(z) \quad (2)$$

$$\sigma_6(x,z) = N_{T1}\Delta[A_{22}Q_{16}(z) - A_{12}Q_{26}(z)] + N_{T2}\Delta[A_{11}Q_{26}(z) - A_{12}Q_{16}(z)] + [M_{T1}^*/(2R\delta^2 A_{11}D_{11}^*)] \times [A_{12}Q_{16}(z) - A_{11}Q_{26}(z)] + (M_{T1}^*/D_{11}^*)zQ_{16}(z)\phi(x) - \beta_6(z)T(z) \quad (3)$$

where

$$\begin{aligned} D_{11}^* &\equiv D_{11} - (B_{11}^2/A_{11});(A_{ij},B_{ij},D_{ij}) \\ &\equiv \int_{-h/2}^{h/2} (1,z,z^2)Q_{ij}dz \\ M_{T1}^* &\equiv M_{T1} - (B_{11}N_{T1}/A_{11});(N_{Ti},M_{Ti}) \\ &= \int_{-h/2}^{h/2} (1,z)\beta_i(z)T(z)dz \\ \beta_i &= \sum_{i=1,2,6} Q_{ij}\alpha_j;\ \phi(x),\psi(x) \equiv e^{-\delta x}(\cos\delta x \pm \sin\delta x) \\ \delta &\equiv (4\Delta A_{11}D_{11}^*R^2)^{-1/4};\ \Delta \equiv (A_{11}A_{22} - A_{12}^2)^{-1} \end{aligned} \quad (4)$$

To obtain the stresses at the outside and inside walls of the shell, one substitutes $z = h/2$ and $z = -h/2$, respectively. In the above equations, the Q_{ij} and α_i are related to the shell coordinate system (1,2 axes). They are obtained from the corresponding quantities relative to the material-symmetry axes (L,T) by means of transformations (A2) and (A3) of Ref. 1 plus the following

$$\begin{aligned} Q_{66} &= (Q_L + Q_T - 2Q_{LT} - 2Q_s)m^2n^2 + Q_s(m^4 + n^4) \\ \begin{Bmatrix} Q_{16} \\ Q_{26} \end{Bmatrix} &= (Q_L - Q_{LT} - 2Q_s)\begin{Bmatrix} m^3n \\ mn^3 \end{Bmatrix} - (Q_T - Q_{LT} - 2Q_s)\begin{Bmatrix} mn^3 \\ m^3n \end{Bmatrix} \\ \alpha_6 &= 2(\alpha_L - \alpha_T)mn,\ m \equiv \cos\theta,\ n \equiv \sin\theta \end{aligned} \quad (5)$$

where Q_L, Q_T, Q_{LT}, Q_s are as defined by Eqs. (A1), Ref. 1.

For the quasi-isotropic case, two different sets of Q_{ij} and α_i are used. In calculating the integrated stiffnesses A_{ij}, B_{ij}, D_{ij}, the transformations given by Eqs. (A4) of Ref. 1 plus the following are used:

$$\begin{aligned} Q_{66} &= (\tfrac{1}{8})(Q_L + Q_T) - (\tfrac{1}{4})(Q_{LT} - 2Q_s) \\ \alpha_1 &= \alpha_2 = (\tfrac{1}{2})(\alpha_L + \alpha_T),\ \alpha_6 = 0 \end{aligned} \quad (6)$$

In calculating the stress components with Eqs. (1–3), Eq. (5) is used to calculate the $Q_{ij}(z)$ and $\alpha_i(z)$ for the particular radial location desired.

The stresses relative to the material-symmetry axes (L,T) are obtained by means of Mohr's stress circle transformations, i.e.,

$$\begin{aligned} \sigma_L(x,z) &= \sigma_1(x,z)m^2 + \sigma_2(x,z)n^2 + 2\sigma_6(x,z)mn \\ \sigma_T(x,z) &= \sigma_1(x,z)n^2 + \sigma_2(x,z)m^2 - 2\sigma_6(x,z)mn \\ \sigma_{LT}(x,z) &= -\sigma_1(x,z)mn + \sigma_2(x,z)mn + \sigma_6(x,z)(m^2 - n^2) \end{aligned} \quad (7)$$

Equations (7) replace Eqs. (A12) of Ref. 1.